A Modeling Framework to Estimate Patellofemoral Joint Cartilage Stress *In Vivo*

THOR F. BESIER[3], GARRY E. GOLD[4], GARY S. BEAUPRÉ[1,2], and SCOTT L. DELP[1,2,3]

[1]VA Rehabilitation Research and Development Center, Palo Alto, CA; and [2]Biomechanical Engineering Division, Departments of [3]Bioengineering, and [4]Radiology, Stanford University Medical Center, Stanford, CA

ABSTRACT

BESIER, T. F., G. E. GOLD, G. S. BEAUPRÉ, and S. L. DELP. A Modeling Framework to Estimate Patellofemoral Joint Cartilage Stress *In Vivo*. *Med. Sci. Sports Med.*, Vol. 37, No. 11, pp. 1924–1930, 2005. **Purpose:** Patellofemoral (PF) pain is common among athletes and may be caused by increased subchondral bone stress as a result of increased stress in the cartilage of the femur or patella. This article presents a modeling pipeline to estimate *in vivo* cartilage stress in the PF joint. **Methods:** The modeling pipeline uses the finite element method to calculate stresses and strains in the PF joint cartilage. Model inputs include an accurate geometrical representation of the bones and cartilage from magnetic resonance imaging (MRI), cartilage material properties, and an estimate of muscle forces from an EMG-driven musculoskeletal model. Validation is performed using PF joint contact area and patellar orientation measured from upright, weight-bearing MRI. Preliminary data from an active, pain-free subject illustrate the modeling pipeline to calculate cartilage stress during a static squat. **Results:** The quasistatic finite element simulation reproduced the orientation of the patella to within 2.1 mm and predicted the PF joint contact area to within 2.3%. Octahedral shear stresses were highest in the central, lateral aspect of the patella cartilage with a peak of 2.5 MPa. The corresponding stresses in the femoral cartilage reached only 2.0 MPa. However, peak hydrostatic pressures were higher within the femoral cartilage (3.5 MPa) than the patellar cartilage (2.3 MPa). **Conclusion:** The methods presented in this article offer a novel approach to calculate PF joint cartilage stress *in vivo*. Future efforts will use this modeling pipeline to further our knowledge of PF pain and potential rehabilitation strategies. **Key Words:** PATELLOFEMORAL PAIN, WEIGHT-BEARING MRI, FINITE ELEMENT MODEL, EMG-DRIVEN MODEL

Patellofemoral (PF) pain is recognized as one of the most common disorders of the knee, accounting for 25% of all knee pain seen in some sports medicine clinics (3,15). Despite its high prevalence, the etiology of PF pain remains unclear. The mechanics of the PF joint are complex, and pain may arise from a variety of structures, including subchondral bone, synovial plicae, infrapatellar fat pad, retinacula, joint capsule, and tendons (8). For those patients for whom the etiology of PF pain cannot be traced to soft-tissue pathologies, a commonly proposed mechanism for PF pain is increased cartilage stress at the PF joint that leads to increased pressure on the subchondral bone, resulting in pain (20). This mechanism is supported by the fact that pain receptors have been isolated in the subchondral bone plate of human patellae (34). However, testing the hypothesis that increased cartilage stress leads to PF pain is difficult due to the inability to experimentally measure the full three-dimensional state of stress within cartilage tissue. The purpose of this study was to develop and test a method to estimate *in vivo* cartilage stress using a subject-specific finite element model of the PF joint.

Address correspondence to: Thor Besier, PhD, Biomechanical Engineering Division, Durand Building, Room 205, Stanford University, Stanford, CA 94305-4038; E-mail: besier@stanford.edu.
Submitted for publication December 2004.
Accepted for publication June 2005.

0195-9131/05/3711-1924/0
MEDICINE & SCIENCE IN SPORTS & EXERCISE®

DOI: 10.1249/01.mss.0000176686.18683.64

Calculating cartilage stress is technically challenging, as many factors can influence stress, including the joint contact force, material properties of the tissue, the geometry of the articulating surfaces, and the cartilage thickness (Fig. 1). Previous researchers (10,31) have calculated average PF joint stress by estimating the joint contact force and dividing this by a contact area measured with magnetic resonance imaging (MRI). This method has been used to illustrate increased average joint stress in PF pain patients compared with active, pain-free controls during walking and stair climbing (10,31). However, a limitation of this approach is that it does not provide information regarding the distribution and peak values of stress across the joint. Stress distribution might be important when considering patients with PF pain, as small regions of high stress could lead to pain and may not be seen if an average stress is calculated. More complex models are required to calculate stress distribution. One approach is to use an elastic foundation contact algorithm or rigid body spring model (1,9,24,26). This approach uses a number of springs across the surface of each bone to prevent penetration of rigid bodies during a dynamic simulation. Other algorithms that account for cartilage deformation have been used to calculate contact pressures in the tibiofemoral joint (6,19) and the PF joint (12,17). One problem with using these spring-contact models is that they only calculate contact pressure and do not calculate the stress distribution throughout the cartilage or the resulting subchondral bone stress. To determine stress and strain fields throughout a complex structure such as the PF joint, the finite element method can be used.

In the finite element method, a complex geometric shape is modeled as a mesh of simpler structures (finite elements),

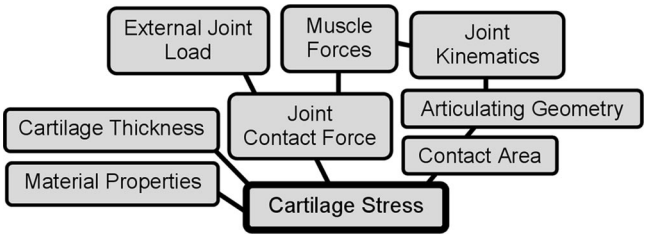

FIGURE 1—Mechanical factors effecting cartilage stress.

each having an appropriate material property. Displacement and/or force boundary conditions are then applied to the model and the subsequent stresses and strains in all elements are computed. The finite element method is well suited to parametric analyses, in which the effect of specific parameters can be investigated in a controlled manner. However, patient-population studies using the finite element method are lacking, partly due to the complexity in creating subject-specific geometries with subject-specific loading conditions. A few finite element models of the PF joint have been developed to calculate the stresses throughout the patella during passive flexion (18,22) and loaded knee flexion (18). Fernandez and Hunter (18) recognized the importance of modeling multiple muscles with physiologic forces to account for different activation patterns. It was concluded that future efforts should focus on integrating muscle EMG to account for subject-specific muscle forces (18). We present a modeling approach that uses an EMG-driven musculoskeletal model to estimate subject-specific muscle forces, which are used as input to a finite element model of the PF joint (see articles by Buchanan et al. and Lloyd et al. in this issue). The long-term goal of this research is to use this modeling pipeline to estimate cartilage stress in a group of PF pain patients to test the hypothesis that these patients have increased cartilage stress compared to pain-free individuals. These advanced methods will allow us to investigate the cartilage stress distribution resulting from different treatment modalities such as muscle strengthening and patellar taping or bracing.

METHODS

The modeling pipeline can be described in three parts: a) create subject-specific geometry and finite element mesh; b) obtain subject-specific joint orientation and muscle forces; and c) perform simulation and test the model. Data were obtained from a physically active, pain-free volunteer to illustrate the modeling process. Before data collection, the subject was informed of all data collection procedures and signed a consent form to comply with the institutional review board of Stanford University.

Creating subject-specific geometry and finite element mesh. Several steps were taken to create subject-specific bone and cartilage geometry and finite element mesh of the PF joint, as illustrated in Figure 2. First, sagittal plane MR images of the knee were acquired with a 1.5-T General Electric (GE Healthcare, Milwaukee, WI) MRI scanner using a fat-suppressed spoiled gradient echo sequence (repetition time (TR): 60 ms, echo time (TE): 5 ms, flip angle (FA): 40°, matrix: 256 × 256, field of view (FOV): 12 ×12 cm, slice thickness: 1.5 mm, scan time 10:25 min; Fig. 2a). During this scan, the subject was supine with the knee fully extended to ensure the cartilage was imaged in an undeformed state.

The MR images were manually segmented using a custom Matlab program (Mathworks, Natick, MA) to obtain a three-dimensional point cloud of the femur, tibia, and patellar including the articular cartilage of the patella and femur (Fig. 2b). The insertion of the quadriceps tendon on the patella and the patellar tendon were also segmented from the images. Triangulated surfaces were then fit to the point clouds (Fig. 2c) using a commercial software package (Raindrop Geomagic, Research Triangle Park, NC) and nonuniform rational B splines (NURBS) fit to the bone and the cartilage surfaces. NURBS surfaces were used to create a uniform mesh of quadrilateral elements for the bone of the patella, femur, and tibia using Patran (MSC.Software Corp., Santa Ana, CA). The femoral and patellar cartilage was represented as three-dimensional hexahedral continuum elements (Fig. 2d).

Obtaining subject-specific joint orientation and muscle forces. Boundary conditions in the finite element model consisted of displacements and forces applied to the

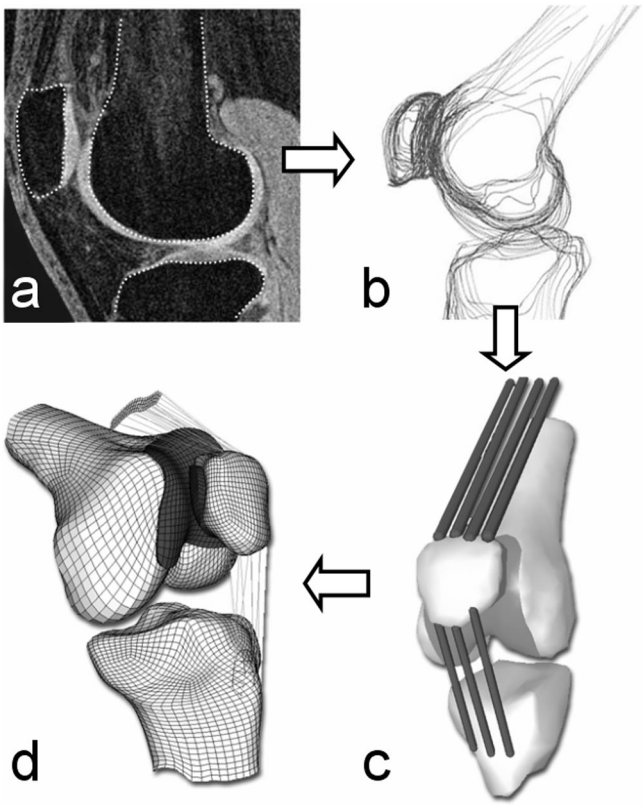

FIGURE 2—Steps to create subject-specific finite element mesh of the patellofemoral joint. Sagittal plane MR images (a) are manually segmented to create a three-dimensional point cloud of the bones and cartilage (b). A triangulated surface is then fit to the point cloud and the geometry of the muscles and tendons are added (c). Nonuniform rational B splines are fit to the surfaces of the bone and cartilage and used to generate quadrilateral and hexahedral meshes of the bones and cartilage (d).

PF joint. For quasistatic loading simulations, we constrained the position of the femur and tibia and applied quadriceps muscle forces to the patella, which had 6 *df*. Thus, the final position of the patella was determined by the forces of the quadriceps, the tension in the patellar ligament, and the contact between the patella and femur (as in (18) and (22)).

To obtain the orientation of the femur and tibia, we acquired sagittal plane images of the knee using an open-configuration MR scanner (0.5-T SP/i MR GE Healthcare Medical Systems). Using a custom-built low friction backrest, the subject was able to perform a static, upright squat with the knee at 60° of flexion (0.45 body weight applied to each leg; Fig. 3). A three-dimensional fast spoiled gradient echo sequence was employed to obtain 2-mm contiguous sagittal plane images of the patellofemoral joint. The scan took 2 min to acquire the complete PF joint using the following parameters: TR: 33 ms, TE: 9 ms, FA: 45°, matrix: 256 × 160 interpolated to 256 × 256, FOV: 20 × 20 cm. Most patients are able to maintain a static squatting posture within the scanner for the duration of the scan.

The segmentation protocol described above was performed to obtain a triangulated surface of the femur, patella, and tibia. The finite element meshes of the femur and tibia were then registered to the bone surfaces in the 0.5-T weight-bearing scan using Raindrop Geomagic. This transformation ensured that the simulation used the weight-bearing position of the femur and tibia. The patellar finite element mesh was also registered to the patellar position from the weight-bearing MR image and then displaced anteriorly by approximately 5 mm to ensure that there was no contact between the patellar and femoral cartilage at the beginning of the simulation.

Quadriceps muscle forces for our cartilage stress calculations were estimated using an EMG-driven model of the knee (27), with subject-specific musculoskeletal geometry. Briefly, the model takes raw EMG and lower limb joint kinematics as input into a modified Hill-type muscle model to calculate muscle forces and net joint moments at the knee (Fig. 4).

To obtain data for input to the EMG-driven model, our subject performed several tasks in the motion analysis laboratory including walking, jogging, stair climbing, and single- and double-leg squatting. The weight-bearing MRI scan was also simulated in the laboratory using the custom-built backrest to replicate the 60° static flexion position. Standard stereophotogrammetry techniques were used to determine joint kinematic and kinetics (Orthotrak, Motion Analysis Corporation, Santa Rosa, CA). Muscle activity was estimated using surface EMG electrodes (MotionLab Systems, Baton Rouge, LA) placed on the following seven muscles crossing the knee: vastus medialis, vastus lateralis, rectus femoris, semimembranosus, biceps femoris, medial gastrocnemius, and lateral gastrocnemius.

A generic lower limb musculoskeletal model of the lower limb (13) was scaled to fit the motion capture data using SIMM (14). This scaled model was used to obtain subject-specific muscle tendon lengths and moment arms for the seven muscles mentioned above as well as vastus interme-

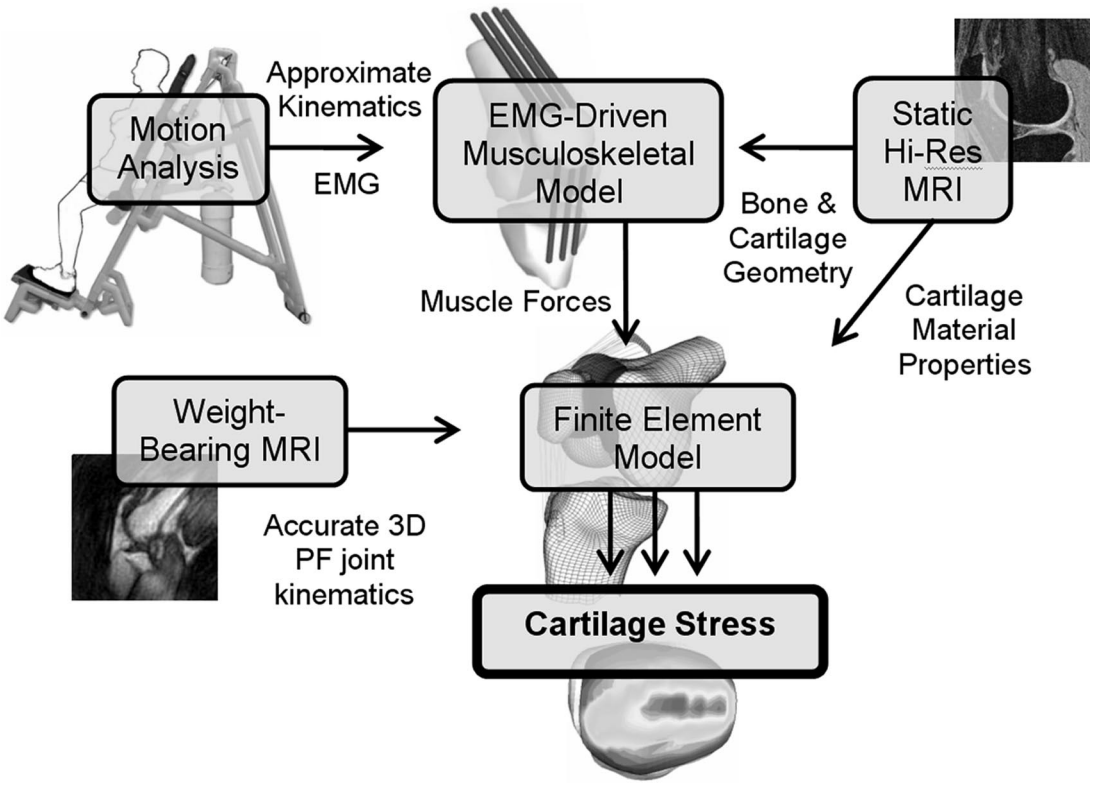

FIGURE 3—Subject performing a static squat within the open-configuration MRI scanner. The custom-built backrest stabilizes the upper body to prevent motion artifact during the 2-min scan. Due to the slight inclination of the backrest, the subject experiences 90% of body weight. Adapted from Gold et al. (21).

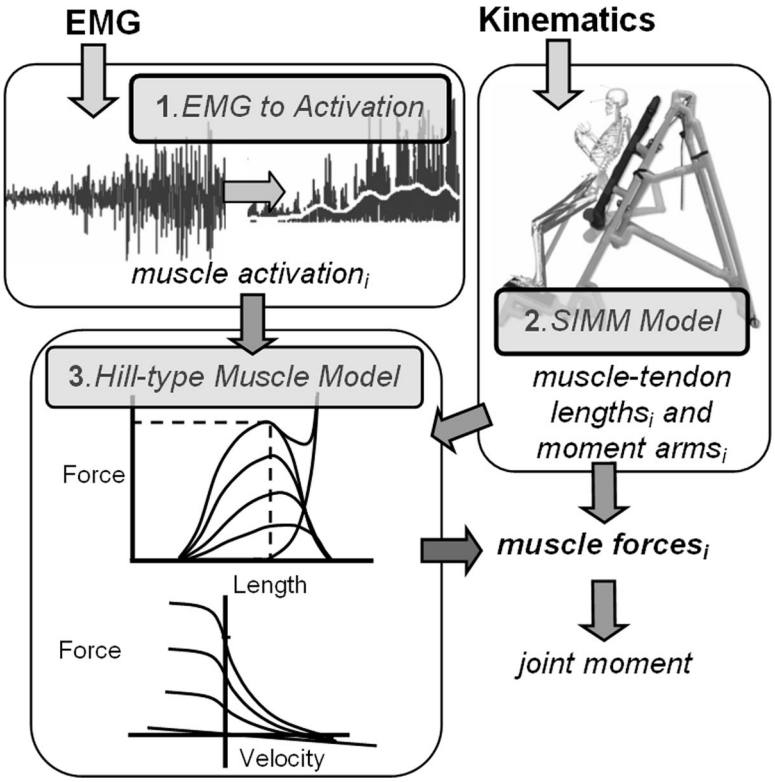

FIGURE 4—The main components of the EMG-driven model. Raw EMG from seven muscles crossing the knee is transformed to an activation time series (1). A scaled musculoskeletal model is created using SIMM (14) with joint kinematics obtained from motion capture data (2). The SIMM model is used to generate muscle tendon lengths and moment arms for each muscle across the knee. Muscle activation and muscle tendon lengths are input to a modified Hill-type muscle model to estimate forces in each muscle crossing the knee (3). Muscle forces can then be multiplied by their respective moment arms and summed to obtain a net joint flexion/extension moment. This moment can be compared to inverse dynamics as a method of validation.

dius and semitendinosus. Muscle tendon lengths for each trial were used as input to the EMG-driven model (27). The model was calibrated to a walk, stair climb, jog, and static squat trial (refer to Buchanan et al. in this issue for more details on this process). Quadriceps muscle forces predicted by the EMG-driven model during the simulated 60° static squat were then used as input to the finite element model.

Perform simulation and test the model. Quasistatic loading simulations were performed using a nonlinear finite element solver (ABAQUS, ABAQUS Inc., Pawtucket, RI). During these simulations, the patella was modeled as a rigid body with 6 *df*. The femur and tibia were also modeled as rigid bodies and their orientation was fixed relative to their position measured from the weight-bearing MRI. Quadriceps muscle forces were applied to the patella such that the patella settled into the trochlear groove of the femur until reaching a state of static equilibrium.

To model the femoral and patellar cartilage, a linear elastic material model was used (23) with an elastic modulus of 6 MPa and a Poisson ratio of 0.47 (4). Linear elastic material models for cartilage are considered appropriate and valid for whole-joint models (12,25) due to the elastic response of cartilage during activities involving loading frequencies greater than 0.1 Hz, such as walking and stair climbing. Nonlinear contact elements were used between the patellar and femoral cartilages to simulate low friction *in vivo* conditions (friction coefficient of 0.001). In this finite element model, the subchondral bone was not explicitly modeled in order to reduce the model complexity. Because subchondral bone is at least two orders of magnitude stiffer than cartilage (5), treating the subchondral bone as rigid has been shown to be a valid approximation (16,25,30). The nodes of the subchondral bone were tied to the nodes of the underlying bone rigid body, allowing for easy registration and/or rotation of the femur, tibia, and patella.

Tension-only elements were used to represent the patellar tendon, which connected the patella rigid body with the tibia rigid body. The elements of the patellar tendon were given a total stiffness of 2000 $N \cdot mm^{-1}$ (32). Nonlinear tendon stiffness (to account for tendon "crimping") was not modeled in this simulation, as the initial orientation of the patella was taken from the weight-bearing MRI, when the patellar tendon was already under tension. The quadriceps muscles were also modeled as tension-only elements, which connected the femur rigid body with the patella. The quadriceps elements were separated into functional groups to represent the rectus femoris (three elements), vastus medialis (six elements), vastus lateralis (six elements), and vastus intermedius (six elements). These muscle groups were actuated based on the forces predicted from the EMG-driven model during the 60° static squat.

To test the finite element model, we compared the final position of the patella from the simulation with the weight-bearing MR images. The contact area between the femur and patella was also measured from the weight-bearing MR images (7) and compared to the contact area predicted by the finite element model. To illustrate changes in patellar cartilage stress distribution that might occur with varying muscle forces, we increased the vastus medialis muscle forces by 20% in one simulation and then increased the vastus lateralis muscle forces by 20% in a second simulation. Finally, another pain-free volunteer was scanned using the same protocol as above to create a second patellofemoral joint model. We used the same cartilage material properties as the previous model and applied

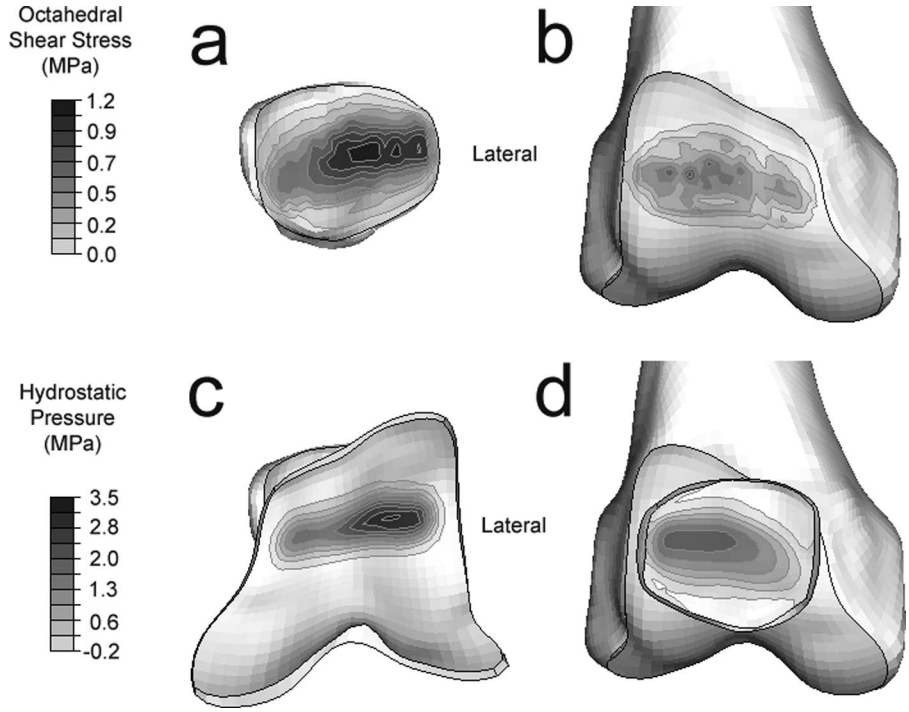

FIGURE 5—Cartilage stress distributions during a static squat with the knee at 60° of flexion. Octahedral shear stress was greater in the patella (a) compared with the femur (b). Hydrostatic pressures on the subchondral surface of the cartilage were higher in the femoral cartilage (c) compared with the patella (d).

the same muscle forces as those obtained from the EMG driven model of the first subject. The purpose of this second simulation was to illustrate the potential stress distribution changes that might occur due to altered joint geometry.

RESULTS

A net knee extension moment of 20.2 N·m was generated by our subject during the 60° squat, as determined by inverse dynamics. The EMG-driven model predicted the following quadriceps muscle forces to produce this net moment; vastus intermedius 226.7 N, vastus lateralis 326.1 N, vastus medialis 195.7 N, and rectus femoris 48.6 N. Applying these forces to the quasistatic finite element simulation resulted in a patella orientation that was 2.1 mm lateral to the patellar position measured from the weight-bearing MR images. The patellofemoral joint contact area predicted from the finite element model was 543 mm^2, which was within 2.3% of the measured contact area from the MRI (556 mm^2).

Octahedral shear stresses were highest on the contacting surface of the patellar cartilage (Fig. 5a), with a maximum stress of 1.16 MPa. The stress was distributed evenly across the central aspect of the patella, with higher stresses on the lateral side compared to the medial side (Fig. 5a). On the corresponding lateral aspect of the femoral cartilage, the octahedral shear stress reached a peak of 0.93 MPa on the surface (Fig. 5b). Octahedral shear stress on the subchondral surface of the cartilage was approximately 40% less than that experienced at the surface of both the femoral and patellar cartilage.

The hydrostatic pressure within the cartilage was distributed evenly throughout the depth of the tissue. Slightly higher pressures were found at the subchondral surface of the patellar and femoral cartilage compared to the contacting surface (<10% difference). Peak hydrostatic pressure was highest in the femoral cartilage (3.45 MPa; Fig. 5c) compared to the patellar cartilage (2.31 MPa; Fig. 5d).

Figure 6 illustrates the change in patellar cartilage octa-

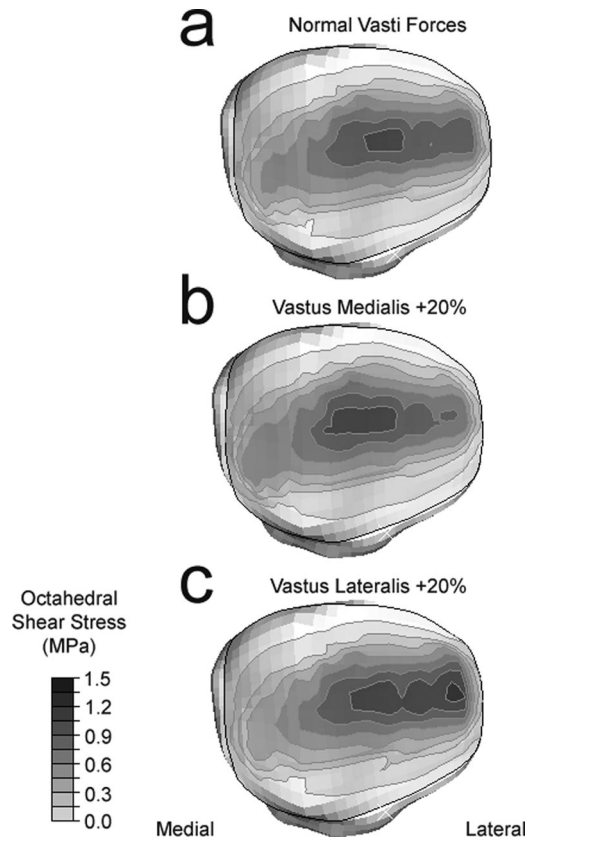

FIGURE 6—Patellar cartilage octahedral shear stress distributions with muscle forces predicted by the EMG-driven model (a) and with increased vastus medialis (b) and vastus lateralis (c) forces.

hedral shear stress with altered vasti muscle forces. As expected, peak cartilage stresses shifted medially with increased vastus medialis muscle forces (Fig. 6b) and laterally with increased vastus lateralis activity (Fig. 6c). Increasing the vastus medialis force by 20% increased the peak octahedral shear stress in the patellar cartilage by approximately 4%. However, increasing the vastus lateralis muscle force by 20% increased the peak octahedral shear stress in the patellar cartilage by 22%.

Applying the same muscle forces to the second patellofemoral joint model (whose geometry was obtained from our second volunteer) resulted in an increase in the peak hydrostatic and octahedral shear stresses in both patellar and femoral cartilage by as much as 22%. The stress distribution was also qualitatively different from the first model. For example, the peak hydrostatic stresses in the patellar cartilage of the first model occurred on the lateral aspect of the patella, whereas the second model had peak hydrostatic patellar cartilage stress in the central region of the patella.

DISCUSSION

The purpose of this study was to develop and test a method to estimate PF joint cartilage stress using the finite element method, with subject-specific input parameters. Finite element models have been extremely useful for understanding stress distributions throughout complex biological structures, but have primarily been used for parametric analyses or theoretical investigations rather than population-based clinical studies. A unique aspect of our modeling pipeline is the use of muscle forces predicted from an EMG-driven model to provide subject-specific loading conditions. Accounting for individual muscle activation patterns is important for understanding changes in cartilage stresses. This is highlighted by the nonuniform increase in patellar cartilage octahedral shear stresses seen between the increased vastus medialis and vastus lateralis loading scenarios. Modeling subject-specific geometry is also important when estimating cartilage stress. We have shown differences in cartilage stress variables as large as 20% when using similar loading cases with different geometry.

The acquisition of weight-bearing MR images is also unique and provides accurate orientation of the bones for the finite element model as well as testing. We have shown that model predictions of patellar orientation and PF joint contact area are close to experimental measures. Although the finite element component of the model may be considered "simple" compared with previous models (18,22), our approach is well suited to understand stress distributions throughout articular cartilage across a wide range of subjects performing different tasks under physiologic loading conditions.

The goal for developing this modeling approach is to gain insight into the mechanism of PF pain, which is hypothesized to relate to pressure placed on pain receptors within the subchondral bone. Our assumption is that stress developed in the cartilage will be transferred directly to the subchondral bone. Making this assumption eliminates the need to model the deformation of the underlying bone, considerably reducing the model complexity. However, this raises an interesting question. What stresses within the cartilage are important to elicit a pain response from nociceptors in the subchondral bone? The subject in this study had large octahedral shear stresses within the patella cartilage yet the greatest hydrostatic pressures were present in the femoral cartilage. Which of these stresses are more important for the sensation of pain? Is it the femoral or patellar cartilage that is important? Pain receptors in the subchondral bone may respond to shear stress just as much as compressive stress. Therefore, measures that combine the effects of compression and shear, such as the osteogenic index (5) or strain energy density (11) might correlate to PF pain.

As with any modeling approach, there are limitations that should be addressed. First, the muscle forces predicted by the EMG-driven model can only be indirectly validated by comparing net joint moments with inverse dynamics (27). However, the results of the finite element model are sensitive to these muscle forces, so the predicted patellar kinematics and PF contact area from the finite element model provide another form of validation for the muscle forces. We have confidence that the muscle forces are reasonable because they predict the orientation of the patella and the PF contact area that are consistent with MRI measurements. Another limitation with our finite element model is that the material properties that we have used to represent cartilage do not take into account time-history or depth-dependent characteristics of the tissue. Because we are interested in modeling activities of daily living that are transient in nature, such as walking, stair climbing, and running, a simplified, elastic cartilage model is justified (12,25). However, we are also using a single value to represent the Young's modulus of the femoral and patellar cartilage. The effective stiffness of cartilage is expected to vary: between individuals, throughout the articular cartilage depth, across the cartilage surface, and between the femur and patella. Quantitative MRI techniques are currently being pursued to measure varying cartilage material properties *in vivo* (33,29) that can be included into our finite element framework. The third limitation of this approach is that the finite element model is quasistatic and therefore estimates cartilage stress during a discrete point in time. Explicit finite element methods may be used to model PF joint dynamics or a hybrid model that combines forward dynamics simulation with the finite element method may prove useful. To model the dynamics of the patella using the finite element method, complexities such as muscle–muscle interactions, muscle–bone contact, and nonlinear patellar tendon properties need to be considered. In anticipation for dynamic models, we are currently developing real-time MRI protocols that are capable of capturing PF joint motion *in vivo* (2,28). This novel scanning technique may be used to calculate PF joint kinematics and test dynamic models of the PF joint.

We thank David Lloyd and Tom Buchanan for their input with the EMG-driven modeling, Chris Powers for his thoughtful comments, and Christie Draper for her help with data collection.

This study received financial support from the Department of Veterans Affairs, Rehabilitation R&D Service (grant A2592R), NIH

EB0002524-01, and Stanford University Regenerative Medicine (1R-90 DK071508).

REFERENCES

1. AN, K. N., S. HIMENSO, H. TSUMARA, T. KAWAI, and E. Y. S. CHAO. Pressure distribution on articular surfaces:application to joint stability analysis. *J.Biomech.* 23:1013–1020, 1990.
2. ASAKAWA, D. S., K. S. NAYAK, S. S. BLEMKER, et al. Real-time imaging of skeletal muscle velocity. *J. Magn. Reson. Imaging* 18:734–739, 2003.
3. BAQUIE, P., and P. BRUKNER. Injuries presenting to an Australian sports medicine centre: a 12-month study. *Clin. J. Sport Med.* 7:28–31, 1997.
4. BEAUPRE, G. S, and D. R. CARTER. Finite element analysis in biomechanics. In: *Biomechanics; Structures and Systems; A Practical Approach.* A. A. Biewener (Ed.). New York: Oxford University Press , 1992, pp. 149–174.
5. BEAUPRE, G. S., S. S. STEVENS, and D. R. CARTER. Mechanobiology in the development, maintenance, and degeneration of articular cartilage. *J. Rehabil. Res. Dev.* 37:145–151, 2000.
6. BEI, Y., and B. J. FREGLY. Multibody dynamic simulation of knee contact mechanics. *Med. Eng. Physics* 26:777–789, 2004.
7. BESIER, T. F., C. E. DRAPER, G. E. GOLD, G. S. BEAUPRÉ, and S. L. DELP. Patellofemoral joint contact area increases with knee flexion and weight-bearing. *J. Orthop. Res.* 23:345–350, 2005.
8. BIEDERT, R. M., and V. SANCHIS-ALFONSO. Sources of anterior knee pain. *Clin. Sports Med.* 21:335–347, 2002.
9. BLANKEVOORT, L., J. H. KUIPER, R. HUISKES, and H. J. GROOTENBOER. Articular contact in a three-dimensional model of the knee. *J. Biomech.* 24:1019–1031, 1991.
10. BRECHTER, J. H., and C. M. POWERS. Patellofemoral joint stress during stair ascent and descent in persons with and without patellofemoral pain. *Gait Posture* 16:115–123, 2002.
11. CARTER, D. R., T. E. ORR, D. P. FYHRIE, and D. J. SCHURMAN. Influences of mechanical stress on prenatal and postnatal skeletal development. *Clin. Orthop.* 219:237–250, 1987.
12. COHEN, Z. A., J. H. HENRY, D. M. MCCARTHY, V. C. MOW, and G. A. ATESHIAN. Computer simulations of patellofemoral joint surgery. Patient-specific models for tuberosity transfer. *Am. J. Sports Med.* 31:87–98, 2003.
13. DELP, S. L., J. P. LOAN, M. G. HOY, F. E. ZAJAC, E. L. TOPP, and J. M. ROSEN. An interactive graphics-based model of the lower extremity to study orthopaedic surgical procedures. *IEEE Trans. Biomed. Eng.* 37:757–767, 1990.
14. DELP, S. L., and J. P. LOAN. A graphics-based software system to develop and analyze models of musculoskeletal structures. *Comput. Biol. Med.* 25:21–34, 1995.
15. DEVEREAUX, M. D., and S. M. LACHMANN. Patello-femoral arthralgia in athletes attending a sports injury clinic. *Br. J. Sports Med.* 18:18–21, 1984.
16. DONAHUE, T. L., M. L. HULL, M. M. RASHID, and C. R. JACOBS. A finite element model of the human knee joint for the study of tibio-femoral contact. *J. Biomech. Eng.* 124:273–280, 2002.
17. ELIAS, J. J., D. R. WILSON, R. ADAMSON, and A. J. COSGAREA. Evaluation of a computational model used to predict the patellofemoral contact pressure distribution. *J. Biomech.* 37:295–302, 2004.
18. FERNANDEZ, J. W., and P. J. HUNTER. An anatomically based patient-specific finite element model of patella articulation: towards a diagnostic tool. *Biomech. Model. Mechanobiol.* 2:139–155, 2004.
19. FREGLY, B. J., Y. BEI, and M. E. SYLVESTER. Experimental evaluation of an elastic foundation model to predict contact pressures in knee replacements. *J. Biomech.* 36:1659–1668, 2003.
20. FULKERSON, J. P., and K. P. SHEA. Mechanical basis for patellofemoral pain and cartilage breakdown. In: *Articular Cartilage and Knee Joint Function: Basic Science and Arthroscopy.* J. W. Ewing (Ed.). New York: Raven Press, 1990, pp. 93–101.
21. GOLD, G. E., T. F. BESIER, C. E. DRAPER, D. S. ASAKAWA, S. L. DELP, and G. S. BEAUPRÉ. Weight-bearing MRI of patellofemoral joint cartilage contact area. *J. Magn. Reson. Imaging.* 20:526–530, 2004.
22. HEEGAARD, J., P. F. LEYVRAZ, A. CURNIER, L. RAKOTOMANANA, and R. HUISKES. The biomechanics of the human patella during passive knee flexion. *J. Biomech.* 28:1265–79, 1995.
23. HIGGINSON, G. R., and J. E. SNAITH. The mechanical stiffness of articular cartilage in confined oscillating compression. *Eng. Med.* 8:11–14, 1979.
24. JOHNSON, K. L. *Contact Mechanics.* Cambridge: Cambridge University Press, 1985, pp. 104–106.
25. LI, G., O. LOPEZ, and H. RUBASH. Variability of a three-dimensional finite element model constructed using magnetic resonance images of a knee for joint contact stress analysis. *J. Biomech. Eng.* 123:341–6, 2001.
26. LI, G., M. SAKAMOTO, and E. Y. S. CHAO. A comparison of different methods in predicting static pressure distribution in articulating joints. *J. Biomech.* 30:635–638, 1997.
27. LLOYD, D. G., and T. F. BESIER. An EMG-driven musculoskeletal model to estimate muscle forces and knee joint moments in vivo. *J. Biomech.* 36:765–776, 2003.
28. NAYAK, K. S., B. A. HARGREAVES, T. F. BESIER, and S. L.DELP. High resolution real-time MRI of knee kinematics. Radiological Society of North America, Chicago, 2003, p. 332.
29. NIEMINEN, M. T., J. TOYRAS, M. S. LAASANEN, J. SILVENNOINEN, H. J. HELMINEN, and J. S. JURVELIN. Prediction of biomechanical properties of articular cartilage with quantitative magnetic resonance imaging. *J. Biomech.* 37:321–328, 2004.
30. PAPAIOANNOU, G., K. YANG, D. FYHRIE, and S. TASHMAN. Validation of a subject-specific finite element model of the human knee developed for in-vivo tibio-femoral contact analysis. Transactions of the Orthopaedic Research Society, San Francisco, 2004, p. 358.
31. POWERS, C. M., S. R. WARD, P. T. CHEN, L. CHAN, and M. R. TERK. The effect of bracing on patellofemoral joint stress during free and fast walking. *Am. J. Sports Med.* 32:224–231, 2004.
32. REEVES, N. D., C. N. MAGANARIS, and M. V. NARICI. Effect of strength training on human patella tendon mechanical properties of older individuals. *J. Physiol.* 548:971–981, 2003.
33. WAYNE, J. S., K. A. KRAFT, K. J. SHIELDS, C. YIN, J. R. OWEN, and D. G. DISLER. MR imaging of normal and matrix-depleted cartilage: correlation with biomechanical function and biochemical composition. *Radiology* 228:493–499, 2003.
34. WOJTYS, E. M., D. N. BEAMAN, R. A. GLOVER, and D. JANDA. Innervation of the human knee joint by substance-P fibers. *Arthroscopy* 6:254–263, 1990.